Biosensors and Bioelectronics 75 (2016) 337–346

Contents lists available at ScienceDirect

Biosensors and Bioelectronics

journal homepage: www.elsevier.com/locate/bios

Substrate binding to cytochrome P450-2J2 in Nanodiscs detected by nanoplasmonic Lycurgus cup arrays

Lisa Plucinski [a,1], Manas Ranjan Gartia [a,1], William R. Arnold [c], Abid Ameen [b], Te-Wei Chang [a], Austin Hsiao [d], Gang Logan Liu [a,*], Aditi Das [c,e,f,**]

[a] Department of Electrical and Computer Engineering, Micro and Nanotechnology Laboratory, University of Illinois at Urbana-Champaign, 208 North Wright Street, Urbana, IL 61801, United States
[b] Department of Materials Science and Engineering, Micro and Nanotechnology Laboratory, University of Illinois at Urbana-Champaign, 208 North Wright Street, Urbana, IL 61801, United States
[c] Department of Biochemistry, University of Illinois at Urbana-Champaign, 208 North Wright Street, Urbana, IL 61801, United States
[d] Department of Bioengineering, Micro and Nanotechnology Laboratory, University of Illinois at Urbana-Champaign, 208 North Wright Street, Urbana, IL 61801, United States
[e] Department of Comparative Biosciences, University of Illinois at Urbana-Champaign, 208 North Wright Street, Urbana, IL 61801, United States
[f] Beckman Institute for Advanced Science and Technology and Department of Bioengineering, University of Illinois at Urbana-Champaign, 208 North Wright Street, Urbana, IL 61801, United States

ARTICLE INFO

Article history:
Received 13 April 2015
Received in revised form
29 June 2015
Accepted 19 July 2015
Available online 29 July 2015

ABSTRACT

Cytochrome P450s are the primary enzymes involved in phase I drug metabolism. They are an important target for early drug discovery research. However, high-throughput drug screening of P450s is limited by poor protein stability and lack of consistent measurement of binding events. Here we present the detection of substrate binding to cytochrome P450–2J2 (CYP2J2), the predominant P450 in the human heart, using a combination of Nanodisc technology and a nanohole plasmonic sensor called nanoplasmonic Lycurgus cup array (nanoLCA). The Nanodisc, a nanoscale membrane bilayer disc, is used to stabilize the protein on the metallic plasmonic surface. Absorption spectroscopy of seven different substrates binding to CYP2J2 in solution showed that they are all type I, resulting in shifting of the protein bands to lower wavelengths (blue shift). Detection on the nanoLCA sensor also showed spectral blue shifts of CYP2J2 following substrate binding. Finite Difference Time Domain (FDTD) electromagnetic simulation suggested that the blue shift on the nanoLCA is because of the hybridization of plasmon polariton Bloch wave and the electronic resonance of the heme group of CYP2J2. We found the plasmonic properties of the nanoLCA sensor to be highly reproducible, which allowed comparisons among the different substrates at different concentrations. Further, due to the unique spectral properties of the nanoLCA sensor, including the transmission of a single color, we were able to perform colorimetric detection of the binding events. These results indicate that a resonance plasmonic sensing mechanism can be used to distinguish between different substrates of the same binding type at different concentrations binding to P450s and that the nanoLCA sensor has the potential to provide consistent high-throughput measurements of this system.

1. Introduction

The development of a high-throughput label-free method for detecting substrate binding to cytochrome P450s would be an important advance in early stage drug discovery research. In addition to their crucial roles in xenobiotic metabolism, P450s are responsible for important drug–drug interactions which can potentially lead to drug toxicity and fluctuations in protein enzymatic activity (Guengerich, 1999, 2008; Rittle and Green, 2010; Whitlock and Denison, 1995). Several challenges limit the ability to screen drug binding to P450s including that the proper expression, isolation, and purification of these proteins at a high yield is labor intensive (Gillam et al., 1993).

Currently drug binding to P450s is detected using absorbance spectroscopic assays in solution (Luthra et al., 2011). Detection is based on the fact that after drug binding P450s can shift the

* Corresponding author.
** Corresponding author at: Department of Comparative Biosciences, Department of Biochemistry, University of Illinois at Urbana-Champaign, 208 North Wright Street, Urbana, IL 61801, United States.
E-mail addresses: loganliu@illinois.edu (G. Logan Liu), aditidas@illinois.edu (A. Das).
[1] These authors contributed equally.

http://dx.doi.org/10.1016/j.bios.2015.07.041
0956-5663/

absorbance peak at 417 nm (Soret band) to either shorter wavelengths (blue shift, type I binding) or to higher wavelengths (red shift, type II binding) (Davydov and Halpert, 2008; Isin and Guengerich, 2006, 2008; Wells et al., 1992). Label-free optical devices, such as the photonic crystal (Ganesh et al., 2007), ring resonator (Iqbal et al., 2010), interferometer (Lin et al., 1997), and surface plasmon resonance (SPR) sensor (Piliarik et al., 2009; Rich and Myszka 2000) are especially promising for surface-based drug screening applications, which increase sensitivity and reduce the required sample amount. However, these techniques remain limited by the complex and bulky external optical systems required for signal generation, detection, and analysis.

In addition to SPR, plasmonic biosensing can be accomplished by localized surface plasmon resonance (LSPR) and extraordinary optical transmission (EOT). In LSPR, the electric field near metal nanoparticles is amplified resulting in strong scattering spectra ideal for applications in protein biosensing (Anker et al., 2008; Baciu et al., 2008; Wu et al., 2012). Unlike SPR, which uses a metallic thin film and prism system, LSPR does not require a complex system in order to couple the light source to the metal dielectric interface (Haes and Van Duyne, 2004). However, the difficulty in fabricating uniform sensors over a large surface area leads to reduced reliability and limited applications. EOT sensors consist of periodic arrays of nanoholes in metallic thin films (Gordon et al., 2008). Transmission through these films is orders of magnitude greater than that predicted by classical aperture theory partially due to the excitation of surface plasmon resonances (Escobedo, 2013). This reliance on SPR has enabled applications including protein binding (Ji et al., 2009), exosome profiling (Im et al., 2014), and virus detection (Yanik et al., 2010). Similar to LSPR, these sensors do not require a complex optical setup, but it is difficult to fabricate uniform devices over a large surface area.

If there is an overlap between the LSPR device resonance and the molecular resonance of a colored adsorbate, then resonance LSPR can result in larger shifts (Haes et al., 2006). Resonance LSPR has been used to detect drug binding to P450s by measuring the spectral shift of the P450 protein after small molecule binding (Zhao et al., 2008, 2006). The ability to distinguish between type I and type II substrates has been demonstrated using silver LSPR sensors fabricated by nanosphere lithography (Das et al., 2009). The further development of LSPR detection of substrate binding to P450s requires wafer-scale nanoplasmonic sensors with minimum defects and therefore consistent spectral properties. In addition, while silver nanoparticles have a higher sensitivity, gold nanoparticles are inert, making them more compatible with high-throughput drug screening (Karlsson and Stahlberg, 1995; Zeng et al., 2011).

Herein we report the application of a gold nanoplasmonic Lycurgus cup array (nanoLCA) sensor to the detection of substrate binding to P450s. The tapered nanohole shape of the nanoLCA has a metal layer (90 nm) at the rim of the holes and at the bottom of the holes (90 nm), providing an intense electromagnetic field at the bottom and top of the nanohole due to LSPR (Gartia et al., 2013). In addition, during deposition, gold nanoparticles form on the tapered cup sidewalls, contributing to LSPR. The periodicity of nanohole structures also provide surface plasmon polariton-Bloch wave (SPP-BW) due to lattice plasmons. The nanoLCA sensor then operates based on a distinct combination of SPP-BW and LSPR plasmonic properties. Due to the high intensity of LSPR by nanoparticle scattering, the nanoLCA transmission spectrum is characterized by a single peak in the entire visible range.

Crucial parameters characterizing the nanoLCA including the deposited metal layer thickness, height, and pitch have been previously optimized to maximize the sensitivity and minimize the full width half maximum (FWHM) of the transmitted resonance peak (Gartia et al., 2013). We have previously reported the sensitivity of the gold nanoLCA to be 247 nm RIU^{-1}, the figure of merit (FOM) to be 3.3 with a FWHM of 75 nm, and the limit of detection (LOD) to be 7.98×10^{-5} RIU. Here sensitivity is defined as $(\frac{\Delta\lambda}{\Delta n})$, FOM is defined as $(\frac{\Delta\lambda}{\Delta \boldsymbol{n}})(\frac{1}{\boldsymbol{\Delta w}})$, and LOD is defined as $(\frac{2\sigma\Delta n}{\Delta\lambda})$ where $\Delta\lambda$ is the shift in the plasmon resonance peak, Δn is the change in the refractive index, Δw is the FWHM of the plasmon resonance peak, and σ is the standard deviation of noise (0.00986 nm) (Gartia et al., 2013; Hsiao et al., 2015).

While the nanoLCA can be applied to measure drug binding to any P450, here the detection of substrate binding to cytochrome P450-2J2 (CYP2J2) is demonstrated. CYP2J2 is the most common P450 found in the human heart and its primary role is the metabolism of arachidonic acid (AA) (Delozier et al., 2007; Wu et al., 1996). This produces epoxyeicosatrienoic acids, which are required for proper cardiovascular function (Spector et al., 2004; Zeldin, 2001). Additionally, CYP2J2 metabolizes drugs, many of which have been shown to be cardiotoxic. Therefore, it is of interest to know what xenobiotics bind to CYP2J2 in order to assess their interference to AA metabolism.

CYP2J2 is found in the heart and is involved in the metabolism of endogenous fatty acids such as AA and 2-arachidonyl glycerol (2-AG) (McDougle et al., 2014, 2013). CYP2J2 is also known to metabolize several drugs and the predominant drugs were chosen for this study (terfenadine, TFN; ebastine, EBA; MSPPOH; danazol, DAN; and doxorubicin, DOX) (Hashizume et al., 2002; Lafite et al., 2007; Lee et al., 2010; McDougle et al., 2014; Zhang et al., 2009).

Small molecule binding to CYPs is typically assessed using spectral shift titrations (Zhao et al., 2008, 2006). We measure the shift of the Soret at 417 nm to higher or lower wavelength. The extent of this shift is dependent on the substrate. We determined the dissociation constants of each substrate from these shifts as explained in the manuscript. We could not do similar studies with DOX as there is severe spectral overlap between DOX and heme absorbance. We show that we can overcome such difficulties using the nanoLCA sensor.

Most eukaryotic P450s are membrane-bound and outside the cellular environment they tend to denature and become unstable both in solution and when immobilized on surfaces (Bayburt and Sligar, 2002, 2003; Sligar, 2003). In order to circumvent this challenge, we use Nanodiscs to stabilize CYP2J2. Nanodiscs consist of nanosized soluble lipid bilayers held together by membrane scaffold proteins (Denisov et al., 2004; Nath et al., 2007). The use of Nanodiscs is critical for this study because they ensure that the CYP2J2 will be immobilized on the nanoLCA sensor surface in an active conformation.

We report the measurement of the spectral change of immobilized CYP2J2-Nanodiscs (CYP2J2-NDs) corresponding to the binding of seven different type I substrates at two different concentrations and the comparison of these results with conventional solution-based absorption spectroscopy. The resonance of the nanoLCA sensor occurs in the visible range, allowing detection by a conventional halogen light source and portable spectrometer. We also report the spectral reliability of the nanoLCA sensor, which allows for the assessment of substrate-dependent and concentration-dependent shifts. Finally, we introduce the use of bright-field microscope images in order to detect substrate binding to CYP2J2-NDs on the nanoLCA device.

2. Materials and methods

2.1. Materials

Human CYP2J2 cDNA was obtained from OriGene (Catalog No. SC321730) and modified (Rich and Myszka 2000). Ampicillin,

arabinose, chloramphenicol, IPTG and Ni-NTA resin were obtained from Gold Biotechnology and Sigma. δ-aminolevulinic acid was bought from Frontier Scientific. 1-palmitoyl-2-oleoyl-sn-glycero-3-phosphocholine (POPC) and 1-hexadecanoyl-2-(9Z-octadecenoyl)-sn-glycero-3-phospho-L serine (POPS) were purchased from Avanti Polar Lipids, Inc. AA, 2-AG, and MSPPOH were purchased from Cayman Chemical. Other drugs were purchased from the following companies: MP Biomedical (Danazol), Santa Cruz Biotechnology (Ebastine), and Gold Biotech (Doxorubicin). UV-curable polymer was purchased from Norland Products (NOA-61). All other materials and reagents used were purchased from Sigma and Fisher Scientific.

2.2. Recombinant expression of CYP2J2 in Escherichia coli

CYP2J2-D34 was expressed and purified according to previous methods (McDougle et al., 2013; Zelasko et al., 2013). Briefly, a starter culture of DH5α *E. coli* cells containing CYP2J2 and pTGro7 chaperonin plasmids were grown in 25 mL of Luria Bertani (LB) media containing the antibiotics chloroamphenicol (20 μg/mL) and ampicillin (100 μg/mL) at 37 °C and 220 rpm overnight. This culture was then used to inoculate 6 × 500 mL of Terrific Broth (TB) containing chloroamphenicol (20 μg/mL) and ampicillin (100 μg/mL). The culture was grown for 2.5 h at 37 °C and 220 rpm. 0.1 mM δ-aminolevulinic acid was added and the culture was grown at 26 °C and 160 rpm until OD_{600} = 1.0 was reached. Cells were induced with 1 mM Isopropyl β-D-1-thiogalactopyranoside (IPTG) and 2 g of arabinose and left to grow for 44 h. The cells were subsequently centrifuged at 8000 rpm and 4 °C for 15 min. using a Sorvall GSA (Thermo Scientific, Pittsburg PA) rotor. The cells were resuspended in a lysis buffer containing 0.1 mM DTT, 0.2 mM phenylmethanesulfonylfluoride (PMSF), and 5 mg DNase, and then lysed via sonication (5 × 30 s on/off cycles). The membrane fraction was isolated using ultracentrifugation at 35,000 rpm and 4 °C for 30 min. with a Ti-45 rotor (Beckman Coulter, Brea, CA). The pellet was resuspended in 0.1 M potassium phosphate buffer (KPi) containing 1.0% (w/v) sodium cholate, 20% glycerol, and 0.2 M NaCl (column buffer) at 4 °C for four hours with stirring in order to extract the protein. The insoluble fraction was removed via a second ultracentrifugation at 35,000 rpm and 4 °C for 30 min. and the supernatant was applied to a Ni-NTA column to purify His-tagged CYP2J2. Protein was eluted using column buffer containing 200 mM imidazole. The yield of the protein was ~200 nmol/L.

2.3. Incorporation of CYP2J2 into Nanodiscs

Nanodiscs were prepared as previously described (McDougle et al., 2013). A lipid mixture of 20:80 POPS:POPC in $CHCl_3$ was dried under a flow of N_2 gas. The dried lipids were then reconstituted in buffer containing 0.1 M KPi (pH 7.4) and 200 mM cholate. Membrane scaffold protein MSP1E3D1 was added (1:130 MSP:lipids) and allowed to incubate for half an hour at 4 °C. Purified CYP2J2 was then added (0.1 M Kpi (pH 7.4), 20% glycerol, and 0.1% cholate) in a 1:10 CYP2J2:MSP ratio and incubated for one more hour before the addition of Amberlite beads to remove the detergent. This mixture was incubated overnight. Discs were purified via size-exclusion chromatography using an Alliance 2695 analytical separation module (Waters, Milford, MA) coupled to a Waters 996 photodiode array detector (Waters) and a Superdex 10/200 column (GE Healthcare).

2.4. Drug binding to CYP2J2-Nanodiscs in solution

Substrate binding was determined by monitoring the Soret shift from 420–390 nm. Absorbance spectra were taken using a Cary Bio 300 UV–vis spectrophotometer (Agilent Technologies, Santa Clara, CA). An initial spectrum of CYP2J2-Nanodiscs in 0.1 M KPi (pH 7.4) was taken at 37 °C. Substrates were then titrated into this cuvette to saturating amounts. Total volume of organics remained < 2% of the initial volume. To correct for the absorbance of the substrates, separate titration experiments were performed using empty Nanodiscs (without CYP2J2), and these readings were subtracted from the CYP2J2-Nanodisc spectra.

2.5. NanoLCA fabrication and characterization

The tapered nanohole array was made using a previously described method (Gartia et al., 2013). Briefly, the plasmonic structures were prepared using a replica molding process. The mold consisting of a two dimensional square array of nanocup structures with a lattice constant of ~350 nm was first prepared on a glass substrate using laser interference lithography. The two-dimensional square array was transferred to a flexible and optically transparent polyethylene terephthalate (PET) film by nanoreplica molding. To prepare the master substrate for transfer, the mold was cleaned and silanized (Repel-silane ES GE Healthcare, Sigma) for 30 min. followed by ethanol and DI water rinse. A 2 mL drop of UV-curable polymer (NOA-61) was evenly spread on the top of the nanocone master and a supporting PET sheet was carefully put on top of the polymer. The master with the polymer and PET sheet was then exposed to UV-light (105 mW cm^{-2}) for 60 s. After curing, the complimentary nanohole structures were transferred onto the polymer, which was peeled off carefully from the master mold to complete the transfer process. In order to make the device surface plasmon active, 90 nm of gold along with a 5 nm titanium adhesive layer was deposited using electron beam deposition (Temescal six pocket E-Beam Evaporator).

2.6. Immobilization of CYP2J2-Nanodiscs on nanoLCA and spectral measurements

A square device with a 2 cm side length was cut from the prepared nanoLCA and it was cleaned with isopropanol (IPA) and DI water followed by rinsing with IPA and drying with N_2. The sensor was then treated with oxygen plasma (PICO plasma cleaner) for 60 s. and four separate circular wells were formed on the surface using PDMS applied with UV curable polymer (NOA-61). Each well held 45 μL of solution. To initiate CYP2J2-ND immobilization, each well was filled with a 10 mM 11-MUA solution in 70% ethanol and incubation was done at room temperature for 24 h. After immersion, each well was washed three times in 70% ethanol followed by drying with N_2. CYP2J2-ND immobilization to the MUA monolayer occurred by EDC activation. Each well was filled with 10 mM EDC and 8 μM CYP2J2-ND in 10 mM potassium phosphate (KPi) buffer. The EDC and protein were mixed immediately before pipetting into the wells in order to minimize EDC self-reaction and CYP2J2-ND cross-linking. The sensor was incubated in the CYP2J2-ND solution for 1 h at 37 °C. After incubation, each well was rinsed three times with DI water and dried with N_2. Illumination and detection of binding events was accomplished with an upright microscope (Olympus BX51, PA, USA) with a halogen light source using a 20X objective and a portable spectrometer (Ocean Optics, Dunedin, FL). Successful immobilization of MUA and CYP2J2-ND was monitored by measuring the red shift in the transmission spectrum for each well of each device.

2.7. Substrate binding to CYP2J2-Nanodiscs on nanoLCA

A device containing four PDMS wells was used for a single substrate. Two of the wells were replicates used for a high concentration of the substrate, one well was used for a low

concentration of the substrate, and the fourth well was used for the vehicle control, which was 10 mM KPi buffer. The seven substrates tested were the fatty acids AA and 2-Arachidonoylglycerol (2-AG), and the drugs doxorubicin (DOX), ebastine, MSPPOH, terfenadine (TFN), and danazol (DAN). Incubation was done for 30 min at 37 °C. The dissociation constants for all drugs with CYP2J2-ND were measured using solution-based titrations and the maximum value was 20 μM. For the high concentration 300 μM was used and for the low concentration we used a value that was half of the measured dissociation constant for each substrate. After incubation, each well was rinsed with DI water three times and dried with N_2 before taking the transmission spectrum.

2.8. Data analysis

The light source transmission spectrum was measured after each binding step. Every transmission spectrum was then normalized with the light source spectrum for that step in order to obtain the transmissivity and was then smoothened by the Loess Method using OriginPro 9.1 (Origin Labs Inc., Northhampton, MA). It is expected that with a binding event there will be a corresponding shift in the plasmon resonance peak as well as a change in the peak intensity. Here the focus is on the spectral shift and not the intensity change; therefore all transmissivity data was normalized to one in order to better visualize the peak shifts. A Gaussian fit was then performed on each peak in order to obtain the plasmon resonance peak wavelength for each step using OriginPro 9.1 (Origin Labs Inc., Northhampton, MA). The solution-based absorbance data was processed using Matlab R2014a (MathWorks Inc, MA) by subtracting the substrate-free spectrum from each titration spectra. The resulting peak and trough differences were then plotted and fitted to the Michaelis–Menten equation using OriginPro 9.1 (Origin Labs Inc., Northhampton, MA).

2.9. FDTD simulation

3D-FDTD (finite difference time domain) electromagnetic numerical computation was performed by using the FDTD software package from Lumerical Solutions. The total simulation region was set to 350 nm × 350 nm × 800 nm. The boundary conditions in the x and y directions were set to be periodic to present the array effect of the nanoLCA device. The perfect matching layer (PML) was applied in the z-directional boundary condition to minimize the simulation error from boundary reflection. The x-axis polarized plane wave was set to propagate normal to the substrate ($-z$ direction). Modeling of the nanostructure was based on dimensions measured by SEM images of the nanoLCA device. The mesh size was set to be 5 nm in order to minimize stair-case and dispersion errors.

3. Results and discussion

3.1. Substrate binding to CYP2J2-Nanodiscs

Detection of substrate binding to CYP2J2-NDs on the nanoLCA sensor required immobilization of CYP2J2-NDs with the active site of CYP2J2 available. Fig. 1(A) shows a schematic of an immobilized CYP2J2-ND on the nanoLCA and Fig. 1(B) shows a schematic of the binding of AA to CY2J2's active site. Fig. 1(C) shows a schematic of a single cup with a low concentration of CYP2J2-ND binding on the nanoLCA surface. The morphology of the nanoLCA device was confirmed by AFM as shown in Fig. 1(D). Overall, the sensor top surface has uniform hole sizes with few defects. After metal deposition, the nanohole diameter is 180 nm and the periodicity of the holes (distance between two neighboring holes) is 350 nm as measured from SEM images and AFM line scans as shown in Figs. S1 and S2.

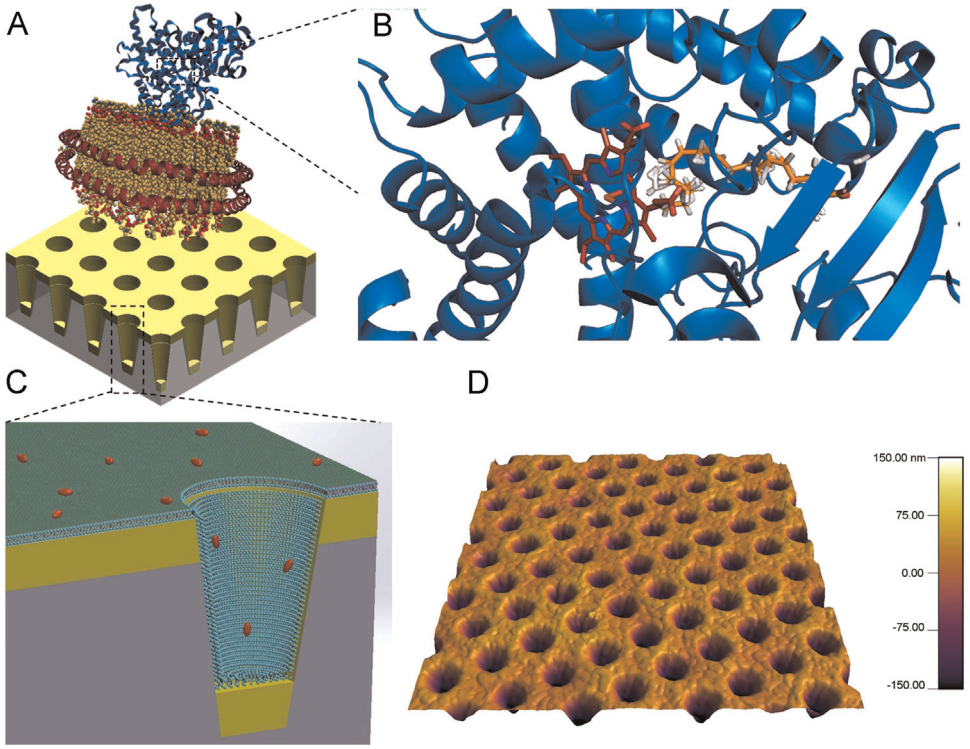

Fig. 1. A schematic of the CYP2J2-ND system (A) with CYP2J2 protein (blue) incorporated into the Nanodisc is shown. The Nanodisc consists of a phospholipid bilayer (gold) and two membrane scaffold proteins (red). (B) Binding of AA to CYP2J2's active site. (C) A schematic of the cross section of a single nanocup with MUA monolayer (light blue) and CYP2J2-ND (red) bound. AFM imaging was used in order to confirm the morphology of the nanoLCA device as shown in (D). (For interpretation of the references to color in this figure legend, the reader is referred to the web version of this article.)

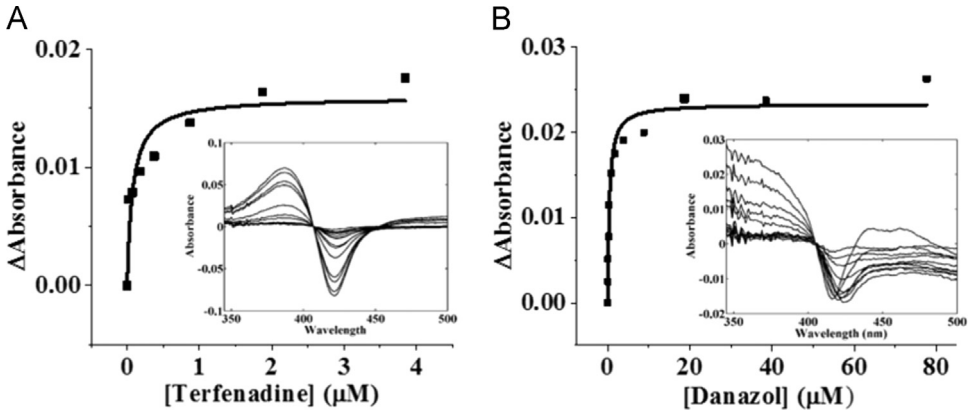

Fig. 2. UV–vis determination of TFN and DAN binding to CYP2J2. Binding was determined by measuring the heme absorbance (Soret) shift to higher wavelengths as the substrate binds and produces a higher spin state of the system. (A) TFN was titrated from 0 to 4 μM and the substrate-free spectrum was subtracted from each titration (inset). The resulting differences of the peaks and troughs were then plotted and fitted to a Michaelis–Menten curve to determine a K_S of 5.6 μM, which approximates K_D. (B) DAN was titrated from 0 to 80 μM and the K_S (1.44 μM) was determined similarly to (A).

The type of binding and dissociation constants of the substrates with CYP2J2-ND were determined by solution-based absorption spectroscopy titration assays. The binding titration data of TFN and DAN with CYP2J2-ND is shown in Fig. 2(A) and (B), respectively. The absorbance difference spectra were measured at varying concentrations of the two drugs. The difference between the peaks and troughs of the absorbance difference spectra were then plotted for the increasing concentrations. The dissociation constants for the two drugs were then determined by fitting the plot to the Michaelis–Menten equation given as $A=\frac{A_{\max}[S]}{K_S+[S]}$, where A is the absorbance, A_{max} is the maximum absorbance, $[S]$ is the concentration of the substrate, and K_S is the spin state constant. For P450s, the dissociation constant, K_D, is approximated by K_S as determined by measuring the absorbance shift as substrates bind near the heme and change the spin state of the iron from low to high spin states in the case of type I binding, resulting in a blue shift in the Soret at 417 nm. Substrates that coordinate the iron of the heme are termed type II substrates and produce characteristic red shifts of Soret at 417 nm. By titration assays, the dissociation constants of the substrates with CYP2J2-ND were found to be 11.3 ± 1.3 μM for AA, 13.1 ± 1.4 μM for 2-AG, 5.6 ± 0.7 μM for ebastine, 10.8 ± 1.5 μM for MSPPOH, 5.6 μM for TFN, and 1.44 μM for DAN. The dissociation constants for AA, 2-AG, ebastine, and MSPPOH with CYP2J2-ND were determined before. (McDougle et al., 2013, 2014). Due to the high absorption of DOX around 417 nm, DOX's signal occludes the heme absorption and the dissociation constant of DOX with CYP2J2-ND cannot be determined by this conventional titration assay.

3.2. Substrate response curves and CYP2J2-Nanodisc surface coverage on nanoLCA sensor

Given these experimental values for the dissociations constants, we determined the response curve for the number of molecules on the sensor surface as a function of concentration of the substrate in solution, as shown in Fig. 3. As can be seen, despite the fact that the dissociation constants for the six measured substrates are the same order of magnitude, there is a detectable difference of the response of CYP2J2-NDs at a wide range of substrate concentrations. The separation between two molecules (d) at a certain concentration was calculated as $d = 1.18C^{\frac{1}{3}}$, where d is in nm and C is in M. At a concentration of ~μM, the distance between two CYP2J2-NDs will be ~118 nm. Therefore, in 1 μM^2 area we can fit about 81 CYP2J2-NDs (assuming a mass of 320 kDa and a minimum diameter of 9 nm for each CYP2J2-ND). The

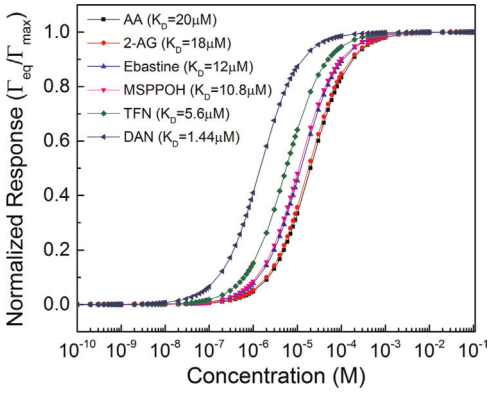

Fig. 3. The response curve for number of molecules on the nanoLCA surface as a function of concentration is shown for the six different substrates with measureable dissociation constants used in this study. The curve is normalized to the maximum number of bound molecules possible.

maximum coverage on our sensor is calculated to be $\Gamma = 383$ pg cm^{-2}, which corresponds to a monolayer of protein covering approximately 50% of the surface. Details of the calculations performed to determine the separation between molecules, CYP2J2-ND molecular weight, and height of CYP2J2-ND/MUA system are given in the Supplementary information.

The binding and unbinding interactions between immobilized CYP2J2-ND and the target drug were modeled with the following equation:

$$\frac{d[\text{CYP2J2–Drug}]}{dt} = k_{on}[\text{CYP2J2}][\text{Drug}] - k_{off}[\text{CYP2J2} - \text{Drug}] \quad (1)$$

where $k_{on}$and k_{off} are the reaction coefficients for binding and release of substrate molecules, respectively. In terms of surface coverage Eq. (2) can be written as:

$$\frac{\partial\Gamma(t)}{\partial t} = k_{on}C[\Gamma_{max} - \Gamma(t)] - k_{off}\Gamma(t) \quad (2)$$

where Γ_{max} is the surface coverage when no more sites are available for substrate binding and C is the concentration of the substrate. Note that k_{on} and k_{off} have different units: M^{-1}s^{-1} for k_{on} and s^{-1} for k_{off}.

Solving Eq. (3) with the boundary condition $\Gamma(0) = 0$ we obtain

$$\Gamma(t) = \frac{k_{on}C\Gamma_{max}}{k_{on}C + k_{off}}[1-\exp\{-(k_{on}C + k_{off})t\}] \quad (3)$$

At equilibrium the rates of binding and release are equal. Hence, with the condition, $\Gamma(t\rightarrow\infty) = \Gamma_{eq}$

Eq. (3) can be written as

$\frac{\Gamma_{eq}}{\Gamma_{mas}} = \frac{C}{C+K_D}$ where K_D is the dissociation constant ($K_D = \frac{k_{off}}{k_{on}}$) approximated as K_S for P450s.

3.3. FDTD simulation of substrate binding to cytochrome P450 in Nanodiscs on the nanoLCA sensor

In order to predict the plasmonic peak shift of P450s on the nanoLCA sensor following substrate binding, FDTD was used to simulate three different conditions, i.e. P450 binding with (1) no substrate, (2) with type I substrate and (3) with type II substrate. The real part of refractive index was calculated from Kramers–Kronig relations for all three cases. The imaginary parts of these three cases, which corresponds to absorption coefficient, are based on measured data and shown in Fig. 4(A). The measured absorbance spectra and the simulated transmission spectra of all three cases are shown in Fig. 4(B) and (C) respectively. It can be observed that the resonance peak at 465 and 605 nm of P450 with no drug binding underwent a blue shift to 462 and 598 nm with the binding of a type I substrate. On the other hand, when a type II substrate was applied to bind on the surface of the nanoLCA, these two resonance peaks were red shifted to 472 and 608 nm. These shifts agrees with previous results (Das et al., 2009). Fig. 4(D) and (F) shows the calculated electric field distribution in *z*-direction for P450, P450 with type I substrate, and P450 with type II substrate, respectively. The electric field for P450 without substrate and with type II substrate are mostly dipolar in nature, whereas for type I substrate, the electric field is quadrupole in nature (Fig. S12). Due to strong charge accumulation on top side of the nanohole rim (Fig. 4(E), the effective dipole moment of the system is increased for the type I substrate case compared to without substrate and with the type II substrate case. The increased dipole moment induces a higher restoring force for the plasmons, which leads to a shift of the plasmon resonance to higher energy (blue shift in the resonance wavelength).

3.4. CYP2J2-Nanodisc immobilization and nanoLCA reliability

A representative red shift in the transmission peak for a single well corresponding to immersion of the nanoLCA sensor in MUA and the CYP2J2-ND/EDC solution is shown in Fig. 5(A). In order to assess the overall success of immobilization and the reliability of the nanoLCA sensor, the average and standard deviation of the plasmon resonance peak wavelength in air was determined for all wells used in this study. The averages and standard deviations of the shifts after MUA and CYP2J2-ND/EDC immersion were also determined. The raw transmission spectra in air for the nanoLCA wells are given in Fig. S5. While between wells there is a variation in intensity, the centroids of the peaks are consistent. The plasmon resonance wavelength in air was 538 ± 2 nm, as shown in Fig. 5(B), with a FWHM of 69 ± 3 nm. Within a single device, the standard deviation of the peak position and FWHM decreases even further as shown in Fig. S6. The shift following MUA immobilization was 2 ± 4 nm and the shift from air following CYP2J2-ND binding was 5 ± 2 nm. The shift for the vehicle control, containing only the 10 mM KPi buffer, never exceeded 1 nm. SEM images and a MATLAB program was used to examine variation of a single sensor on the microscale. SEM images used for the analysis along with histograms of hole diameter and periodicity are shown in Figs. S7–S11.

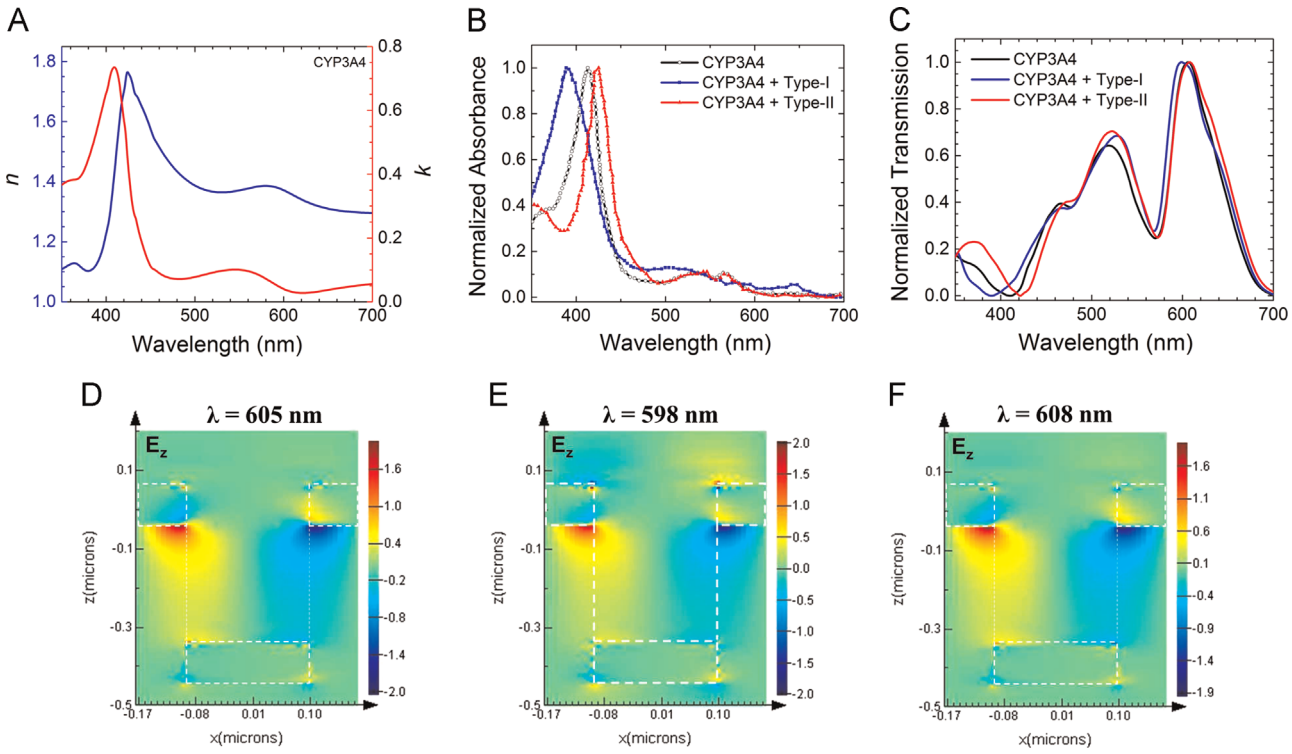

Fig. 4. FDTD simulation of P-450 and substrate system (type I and type II) on top of the nanoLCA. (A) Real (n) and imaginary (k) part of the refractive index of CYP3A4 used for the electromagnetic (FDTD) simulation. (B) Normalized absorbance spectra of CYP3A4 obtained experimentally, before and after substrate binding. The black spectrum is for CYP3A4 without any substrate, the blue spectrum is for CYP3A4 with type I substrate showing blue shift of the peak resonance wavelength position, and the red spectrum is for CYP3A4 with type II substrate showing red shift of the peak resonance wavelength position. (C) Transmission spectra obtained from FDTD simulation showing CYP3A4 before (black), and after substrate binding (blue curve is for type I substrate and red curve is for type II substrate). (D and F) Calculated electric field in *z*-direction for CYP3A4 (D), for CYP3A4 with type I substrate (E), and for CYP3A4 with type II substrate (F).

Table 1
Substrate binding to CYP2J2-NDs in solution and on the nanoLCA sensor. The binding type and dissociation constants were determined using the spectral titration shift method typical for CYPs. The direction of the plasmonic shift corroborates the binding type (type I). Concentration-dependent plasmonic shifts are given as high and low concentrations.

Drug	Binding type	Dissociation constant (μM)	Direction of plasmonic shift	Plasmonic shift (High conc.)	Plasmonic shift (Low conc.)
AA	Type I	20	Blue	14.5 ± 5	8.6
2-AG	Type I	18	Blue	7.2 ± 0.2	4.4
Ebastine	Type I	12	Blue	7.3 ± 0.9	4.8
MSPPOH	Type I	10.8	Blue	6.8 ± 1.7	1.7
TFN	Type I	5.6	Blue	3.7 ± 0.1	2.7
DAN	Type I	1.44	Blue	3.1	2.2
DOX	Type I	Unknown	Blue	7.8 ± 1	7

3.5. Spectral shifts of CYP2J2-Nanodiscs after substrate binding

Table 1 gives a summary of the seven substrates tested for their solution-based and surface-based binding with CYP2J2-NDs. From the solution-based absorbance data, it was determined that all seven substrates (AA, 2-AG, ebastine, MSPPOH, TFN, DAN, and DOX) result in a blue shift in the Soret band of CYP2J2-ND and therefore are classified as type I substrates for this cytochrome P450 protein. As expected for type I substrates, the spectral shift of immobilized CYP2J2-ND on the nanoLCA sensor following substrate binding was consistently to lower wavelengths (blue shift). Despite the fact that the dissociation constants of the seven substrates used here are similar, substrate-dependent shifts were measured in addition to concentration-dependent blue shifts. Fig. 5(C) shows a representative blue shift in the transmission spectrum plasmon resonance peak of CYP2J2-NDs immobilized on

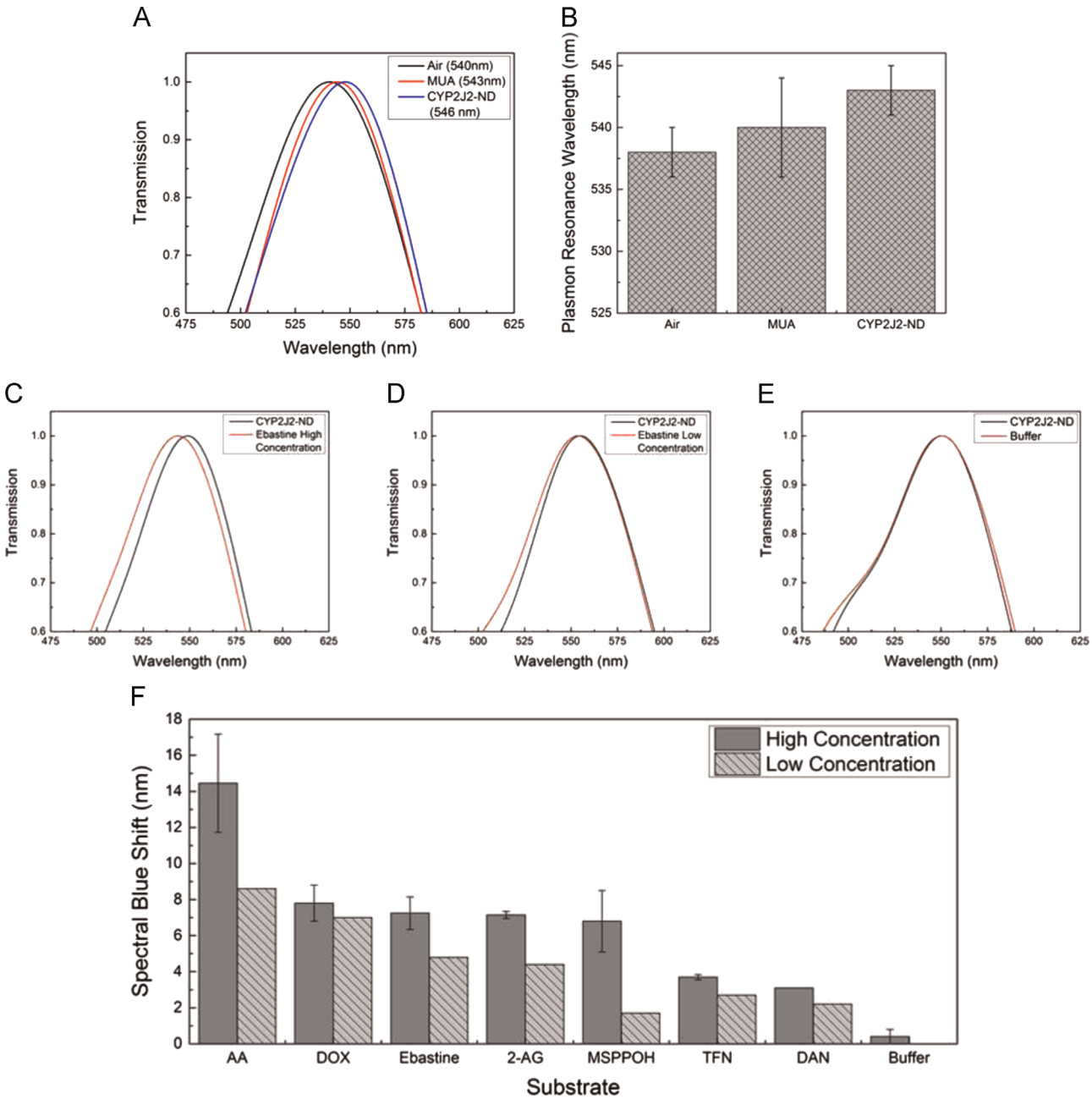

Fig. 5. (A) A representative red shift in the transmission spectra following MUA immobilization and CYP2J2-ND binding with the peak wavelength at each step noted in the legend. (B) A bar graph showing the average plasmon resonance peak wavelength across all wells. The spectral blue shift from a high (C) and low (D) concentration of ebastine binding with immobilized CYP2J2-ND along with the shift corresponding to 10 mM KPi buffer alone (E). The lower panel bar graph shows the shifts on the nanoLCA corresponding to seven different type I substrates at high and low concentrations (F). The high concentration bar corresponds to the average of the two wells with an error bar denoting the standard deviation.

the nanoLCA sensor following immersion in a solution containing a high concentration of ebastine. For comparison, Fig. 5(D) and (E) show the shift after immersion in a low concentration of ebastine and the 10 mM KPi buffer, respectively. The lower concentration of the substrate leads to a lower magnitude spectral blue shift on the nanoLCA and incubation in the KPi buffer alone does not lead to a detectable shift. Additional transmission spectra are shown for AA, 2-AG, and MSPPOH in Fig. S13. Fig. 5(F) shows a bar graph summary of the blue shifts corresponding to substrate binding to CYP2J2-NDs on the nanoLCA sensor for all seven substrates at high and low concentrations.

3.6. Colorimetric detection of substrate binding to CYP2J2-Nanodiscs

The nanoLCA sensor has a single transmission peak in the visible range and therefore bright-field microscope images can be used to detect spectral shifts following substrate binding. In order to carry out the image analysis, the original image of 2048 × 2048 pixels with 24 bit depth was first converted to an 8 bit image by separating the red, green, and blue channels in ImageJ software. Fig. 6(A) shows the intensity of the green channel for MUA, CYP2J2-ND, and ebastine binding in sequence on the nanoLCA false colored in the intensity ranges of 0-255. The average intensity of the red, green, and blue color channels for MUA, CYP2J2-ND, and ebastine is shown in Fig. 6(B). All three color channels follow a similar pattern showing an overall intensity increase. Fig. 6 (C) shows the intensity percentage, calculated as the average intensity of each color channel divided by the sum of the average intensity for each color channel. It can be seen that from MUA to CYP2J2-ND there is a detectable increase in the red and green intensity percentages and a detectable decrease in the blue intensity percentage between the images. These changes in the intensity percentages of the red, green, and blue color channels match what would be predicted for a spectral red shift on the nanoLCA device, corresponding to the spectral data we collected for CYP2J2-ND binding to immobilized MUA. From CYP2J2-ND to ebastine, there is a detectable decrease in the red intensity percentage and a detectable increase in the green intensity percentage. The changes in the color channel intensity percentages indicate that a blue shift is occurring on the nanoLCA device, confirming the spectral data we collected for ebastine binding to CYP2J2-ND. The potential use of the nanoLCA sensor for detecting drug binding to P450s by image analysis alone could drastically improve assay speed allowing high-throughput screening of hundreds of drugs binding to P450s simultaneously.

3.7. Discussion of detection of substrate binding to CYP2J2-Nanodiscs on nanoLCA

Overall, these results suggest that the nanoLCA sensor allows spectral and colorimetric analysis of substrate binding to CYP2J2-NDs that can be carried out using a bright-field microscope, camera, and portable spectrometer. The development of a platform for high-throughput screening of drug binding to P450s will require a device with a small footprint, low cost, sensitive detection, and that can allow parallel detection of hundreds of different drugs at different concentrations. Nanoplasmonic sensors are an excellent candidate since they can be easily miniaturized. In particular, nanohole sensors only require a light source and portable spectrometer for data acquisition. The spectral reliability of the nanoLCA sensor that we have reported here potentially allows quantitative detection of the binding of different substrates at different concentrations to P450s. We have shown that our method can be used to detect different substrates of the same binding type. A FDTD simulation study confirmed the spectral blue shift of type I binding on the nanoLCA device. In addition, we have also presented the potential to use the nanoLCA device to perform colorimetric detection of substrate binding to CYP2J2-NDs due to its distinct spectral properties. This technology should also be reusable with substrates that bind in equilibrium, as it would only require washing with buffer to unbind them.

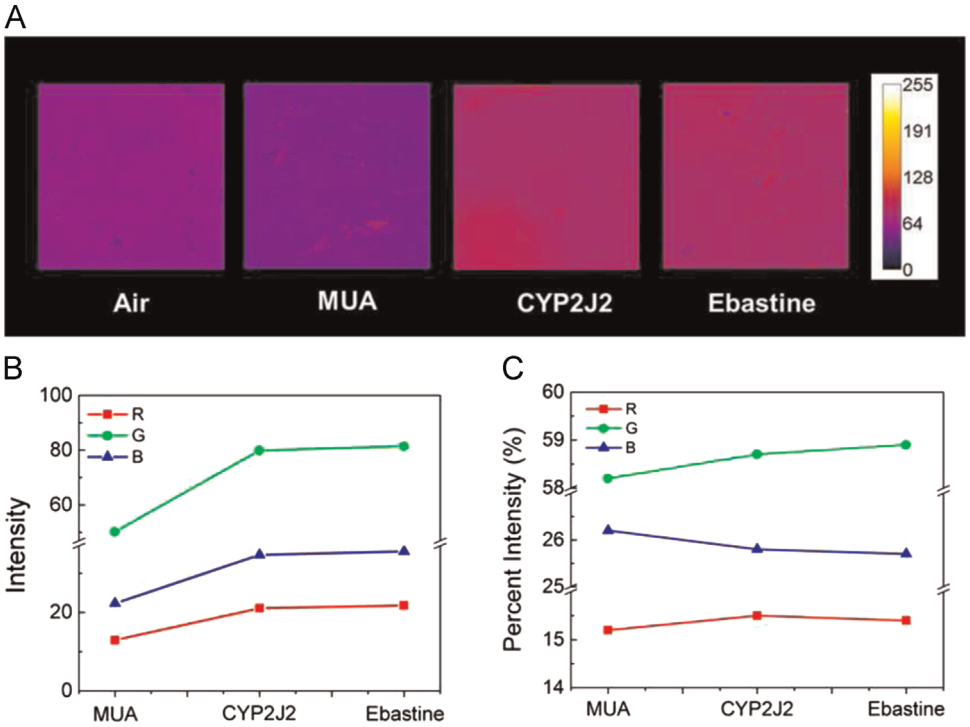

Fig. 6. (A) Images of the green channel intensity for Air, MUA, CYP2J2-ND, and ebastine. The changes in average intensity for the three color channels for MUA, CYP2J2-ND, and ebastine are plotted in (B) and the percent intensity, calculated as the average intensity of the color channel divided by the total average intensity for the image, is plotted in (C).

4. Conclusion

Here we have reported the application of a nanoLCA sensor to the detection of substrate binding to CYP2J2-NDs. The nanoLCA fabrication method relies on wafer-scale nanoreplica molding, which results in uniform sensors with minimal defects. We found the spectral properties of the nanoLCA sensor to be highly reliable, which allowed the detection of substrate dependent and concentration dependent blue shifts, corresponding to the binding of type I substrates to CYP2J2-NDs. Our results were confirmed by traditional solution-based absorption spectroscopy and a FDTD simulation study. We also demonstrated the ability to use brightfield microscope images alone to extract spectral information, based on the fact that the nanoLCA spectrum consists of a single transmission peak in the visible. This study indicates that the nanoLCA sensor has a strong potential for the future development of a high-throughput spectroscopic on-chip method for detecting drug binding to cytochrome P450 proteins.

Author contributions

LP and MRG fabricated sensors, did the experiments, analyzed the data and wrote the manuscript. WRA prepared the protein samples, performed the titration measurements, analyzed the data and wrote the paper, AA performed the microfluidics and did the data analysis, TWC did the simulation studies and wrote the paper, AH did the preliminary experiments, GGL and AD supervised the research and wrote the manuscript.

Acknowledgements

The authors thank Snehita Sri Varma for the preparation of P450 protocol and help in the initial experiments. We thank Daniel McDougle for helpful discussions. We also want to thank Sligar lab for providing the clone for membrane scaffold protein. We thank Prof. Bagchi and Prof. Ferguson for use of their equipment. The authors also thank Xiangfei Zhou for the schematic figures. We thank Hoang Nguyen, Cindy Larson, and Tiziana Bond of Lawrence Livermore National Laboratory for preparation of the master nanopillar mold. We thank National Science Foundation IGERT 0903622 for funding Lisa Plucinski. We want to thank American Heart Association for funding Aditi Das [15SDG25760064].

Appendix A. Supplementary material

Supplementary data associated with this article can be found in the online version at http://dx.doi.org/10.1016/j.bios.2015.07.041.

References

Anker, J.N., Hall, W.P., Lyandres, O., Shah, N.C., Zhao, J., Van Duyne, R.P., 2008. Biosensing with plasmonic nanosensors. Nat. Mater. 7 (6), 442–453.
Baciu, C.L., Becker, J., Janshoff, A., Sonnichsen, C., 2008. Protein-membrane interaction probed by single plasmonic nanoparticles. Nano Lett. 8 (6), 1724–1728.
Bayburt, T.H., Sligar, S.G., 2002. Single-molecule height measurements on microsomal cytochrome P450 in nanometer-scale phospholipid bilayer disks. Proc. Natl. Acad. Sci. USA 99 (10), 6725–6730.
Bayburt, T.H., Sligar, S.G., 2003. Self-assembly of single integral membrane proteins into soluble nanoscale phospholipid bilayers. Protein Sci. 12 (11), 2476–2481.
Das, A., Zhao, J., Schatz, G.C., Sligar, S.G., Van Duyne, R.P., 2009. Screening of type I and II drug binding to human cytochrome P450-3A4 in nanodiscs by localized surface plasmon resonance spectroscopy. Anal. Chem. 81 (10), 3754–3759.
Davydov, D.R., Halpert, J.R., 2008. Allosteric P450 mechanisms: multiple binding sites, multiple conformers or both? Expert Opin. Drug Metab. Toxicol. 4 (12), 1523–1535.
Delozier, T.C., Kissling, G.E., Coulter, S.J., Dai, D., Foley, J.F., Bradbury, J.A., Murphy, E., Steenbergen, C., Zeldin, D.C., Goldstein, J.A., 2007. Detection of human CYP2C8, CYP2C9, and CYP2J2 in cardiovascular tissues. Drug Metab. Dispos. 35 (4), 682–688.
Denisov, I.G., Grinkova, Y.V., Lazarides, A.A., Sligar, S.G., 2004. Directed self-assembly of monodisperse phospholipid bilayer Nanodiscs with controlled size. J. Am. Chem. Soc. 126 (11), 3477–3487.
Escobedo, C., 2013. On-chip nanohole array based sensing: a review. Lab Chip 13 (13), 2445–2463.
Ganesh, N., Zhang, W., Mathias, P.C., Chow, E., Soares, J.A., Malyarchuk, V., Smith, A. D., Cunningham, B.T., 2007. Enhanced fluorescence emission from quantum dots on a photonic crystal surface. Nat. Nanotechnol. 2 (8), 515–520.
Gartia, M.R., Hsiao, A., Pokhriyal, A., Seo, S., Kulsharova, G., Cunningham, B.T., Bond, T.C., Liu, G.L., 2013. Colorimetric plasmon resonance imaging using nano Lycurgus cup arrays. Adv. Opti. Mater. 1 (1), 68–76.
Gillam, E.M., Baba, T., Kim, B.R., Ohmori, S., Guengerich, F.P., 1993. Expression of modified human cytochrome P450 3A4 in *Escherichia coli* and purification and reconstitution of the enzyme. Arch. Biochem. Biophys. 305 (1), 123–131.
Gordon, R., Sinton, D., Kavanagh, K.L., Brolo, A.G., 2008. A new generation of sensors based on extraordinary optical transmission. Acc. Chem. Res. 41 (8), 1049–1057.
Guengerich, F.P., 1999. Cytochrome P-450 3A4: regulation and role in drug metabolism. Annu. Rev. Pharmacol. Toxicol. 39, 1–17.
Guengerich, F.P., 2008. Cytochrome p450 and chemical toxicology. Chem. Res. Toxicol. 21 (1), 70–83.
Haes, A.J., Van Duyne, R.P., 2004. A unified view of propagating and localized surface plasmon resonance biosensors. Anal. Bioanal. Chem. 379 (7–8), 920–930.
Haes, A.J., Zou, S., Zhao, J., Schatz, G.C., Van Duyne, R.P., 2006. Localized surface plasmon resonance spectroscopy near molecular resonances. J. Am. Chem. Soc. 128 (33), 10905–10914.
Hashizume, T., Imaoka, S., Mise, M., Terauchi, Y., Fujii, T., Miyazaki, H., Kamataki, T., Funae, Y., 2002. Involvement of CYP2J2 and CYP4F12 in the metabolism of ebastine in human intestinal microsomes. J. Pharmacol. Exp. Ther. 300 (1), 298–304.
Hsiao, A., Gartia, M.R., Chang, T.-W., Wang, X., Khumwan, P., Liu, G.L., 2015. Colorimetric plasmon resonance microfluidics on nanohole array sensors. Sens. Bio-Sens. Res. 5 (0), 24–32.
Im, H., Shao, H., Park, Y.I., Peterson, V.M., Castro, C.M., Weissleder, R., Lee, H., 2014. Label-free detection and molecular profiling of exosomes with a nano-plasmonic sensor. Nat. Biotechnol. 32 (5), 490–495.
Iqbal, M., Gleeson, M.A., Spaugh, B., Tybor, F., Gunn, W.G., Hochberg, M., Baehr-Jones, T., Bailey, R.C., Gunn, L.C., 2010. Label-free biosensor arrays based on ailicon ring resonators and high-speed optical scanning instrumentation. IEEE J. Sel. Top. Quantum Electron. 16 (3), 654–661.
Isin, E.M., Guengerich, F.P., 2006. Kinetics and thermodynamics of ligand binding by cytochrome P450 3A4. J. Biol. Chem. 281 (14), 9127–9136.
Isin, E.M., Guengerich, F.P., 2008. Substrate binding to cytochromes P450. Anal. Bioanal. Chem. 392 (6), 1019–1030.
Ji, J., Yang, J.C., Larson, D.N., 2009. Nanohole arrays of mixed designs and microwriting for simultaneous and multiple protein binding studies. Biosens. Bioelectron. 24 (9), 2847–2852.
Karlsson, R., Stahlberg, R., 1995. Surface plasmon resonance detection and multispot sensing for direct monitoring of interactions involving low-molecular-weight analytes and for determination of low affinities. Anal. Biochem. 228 (2), 274–280.
Lafite, P., Andre, F., Zeldin, D.C., Dansette, P.M., Mansuy, D., 2007. Unusual regioselectivity and active site topology of human cytochrome P450 2J2. Biochemistry 46 (36), 10237–10247.
Lee, C.A., Neul, D., Clouser-Roche, A., Dalvie, D., Wester, M.R., Jiang, Y., Jones 3rd, J.P., Freiwald, S., Zientek, M., Totah, R.A., 2010. Identification of novel substrates for human cytochrome P450 2J2. Drug Metab. Dispos. 38 (2), 347–356.
Lin, V.S., Motesharei, K., Dancil, K.P., Sailor, M.J., Ghadiri, M.R., 1997. A porous silicon-based optical interferometric biosensor. Science 278 (5339), 840–843.
Luthra, A., Denisov, I.G., Sligar, S.G., 2011. Spectroscopic features of cytochrome P450 reaction intermediates. Arch. Biochem. Biophys. 507 (1), 26–35.
McDougle, D.R., Kambalyal, A., Meling, D.D., Das, A., 2014. Endocannabinoids anandamide and 2-arachidonoylglycerol are substrates for human CYP2J2 epoxygenase. J. Pharmacol. Exp. Ther. 351 (3), 616–627.
McDougle, D.R., Palaria, A., Magnetta, E., Meling, D.D., Das, A., 2013. Functional studies of N-terminally modified CYP2J2 epoxygenase in model lipid bilayers. Protein Sci. 22 (7), 964–979.
Nath, A., Atkins, W.M., Sligar, S.G., 2007. Applications of phospholipid bilayer nanodiscs in the study of membranes and membrane proteins. Biochemistry 46 (8), 2059–2069.
Piliarik, M., Vaisocherova, H., Homola, J., 2009. Surface plasmon resonance biosensing. Methods Mol. Biol. 503, 65–88.
Rich, R.L., Myszka, D.G., 2000. Advances in surface plasmon resonance biosensor analysis. Curr Opin. Biotechnol. 11 (1), 54–61.
Rittle, J., Green, M.T., 2010. Cytochrome P450 compound I: capture, characterization, and C-H bond activation kinetics. Science 330 (6006), 933–937.
Sligar, S.G., 2003. Finding a single-molecule solution for membrane proteins. Biochem. Biophys. Res. Commun. 312 (1), 115–119.
Spector, A.A., Fang, X., Snyder, G.D., Weintraub, N.L., 2004. Epoxyeicosatrienoic acids (EETs): metabolism and biochemical function. Prog. Lipid Res. 43 (1), 55–90.
Wells, A.V., Li, P., Champion, P.M., Martinis, S.A., Sligar, S.G., 1992. Resonance Raman investigations of Escherichia coli-expressed Pseudomonas putida cytochrome

P450 and P420. Biochemistry 31 (18), 4384–4393.
Whitlock Jr., J., Denison, M., 1995. Induction of Cytochrome P450 Enzymes That Metabolize Xenobiotics. In: de Montellano, P.O. (Ed.), Cytochrome P450. Springer, US, pp. 367–390.
Wu, H.J., Henzie, J., Lin, W.C., Rhodes, C., Li, Z., Sartorel, E., Thorner, J., Yang, P., Groves, J.T., 2012. Membrane-protein binding measured with solution-phase plasmonic nanocube sensors. Nat. Methods 9 (12), 1189–1191.
Wu, S., Moomaw, C.R., Tomer, K.B., Falck, J.R., Zeldin, D.C., 1996. Molecular cloning and expression of CYP2J2, a human cytochrome P450 arachidonic acid epoxygenase highly expressed in heart. J. Biol. Chem. 271 (7), 3460–3468.
Yanik, A.A., Huang, M., Kamohara, O., Artar, A., Geisbert, T.W., Connor, J.H., Altug, H., 2010. An optofluidic nanoplasmonic biosensor for direct detection of live viruses from biological media. Nano Lett. 10 (12), 4962–4969.
Zelasko, S., Palaria, A., Das, A., 2013. Optimizations to achieve high-level expression of cytochrome P450 proteins using *Escherichia coli* expression systems. Protein Expr. Purif. 92 (1), 77–87.
Zeldin, D.C., 2001. Epoxygenase pathways of arachidonic acid metabolism. J. Biol. Chem. 276 (39), 36059–36062.
Zeng, S., Yong, K.-T., Roy, I., Dinh, X.-Q., Yu, X., Luan, F., 2011. A review on functionalized gold nanoparticles for biosensing applications. Plasmonics 6 (3), 491–506.
Zhang, Y., El-Sikhry, H., Chaudhary, K.R., Batchu, S.N., Shayeganpour, A., Jukar, T.O., Bradbury, J.A., Graves, J.P., DeGraff, L.M., Myers, P., Rouse, D.C., Foley, J., Nyska, A., Zeldin, D.C., Seubert, J.M., 2009. Overexpression of CYP2J2 provides protection against doxorubicin-induced cardiotoxicity. Am. J. Physiol. Heart Circ. Physiol. 297 (1), H37–H46.
Zhao, J., Das, A., Schatz, G.C., Sligar, S.G., Van Duyne, R.P., 2008. Resonance localized surface plasmon spectroscopy: sensing substrate and inhibitor binding to cytochrome P450. J. Phys. Chem. C 112 (34), 13084–13088.
Zhao, J., Das, A., Zhang, X., Schatz, G.C., Sligar, S.G., Van Duyne, R.P., 2006. Resonance surface plasmon spectroscopy: low molecular weight substrate binding to cytochrome P450. J. Am. Chem. Soc. 128 (34), 11004–11005.